An analytic secondary source model of edge diffraction impulse responses

U. Peter Svensson[a] and Roger I. Fred[b]
Department of Applied Acoustics, Chalmers University of Technology, SE-412 96 Göteborg, Sweden

John Vanderkooy
Audio Research Group, Department of Physics, University of Waterloo, Waterloo, Ontario N2L 3G1, Canada

(Received 14 July 1997; revised 18 June 1999; accepted 19 July 1999)

A new impulse-response model for the edge diffraction from finite rigid or soft wedges is presented which is based on the exact Biot–Tolstoy solution. The new model is an extension of the work by Medwin *et al.* [H. Medwin *et al.*, J. Acoust. Soc. Am. **72**, 1005–1013 (1982)], in that the concept of secondary edge sources is used. It is shown that analytical directivity functions for such edge sources can be derived and that they give the correct solution for the infinite wedge. These functions support the assumption for the first-order diffraction model suggested by Medwin *et al.* that the contributions to the impulse response from the two sides around the apex point are exactly identical. The analytical functions also indicate that Medwin's second-order diffraction model contains approximations which, however, might be of minor importance for most geometries. Access to analytical directivity functions makes it possible to derive explicit expressions for the first- and even second-order diffraction for certain geometries. An example of this is axisymmetric scattering from a thin circular rigid or soft disc, for which the new model gives first-order diffraction results within 0.20 dB of published reference frequency-domain results, and the second-order diffraction results also agree well with the reference results. Scattering from a rectangular plate is studied as well, and comparisons with published numerical results show that the new model gives accurate results. It is shown that the directivity functions can lead to efficient and accurate numerical implementations for first- and second-order diffraction.
[S0001-4966(99)02111-6]

PACS numbers: 43.20.Bi, 43.20.Fn, 43.20.Px [DEC]

INTRODUCTION

The classic problem of edge diffraction from an infinite wedge irradiated by a point source has explicit impulse-response (IR) solutions for the cases of a rigid wedge and a pressure-release wedge. These were presented by Biot and Tolstoy in 1957,[1] but few studies employed these solutions until Medwin applied them to underwater and noise-barrier cases.[2] Comparisons of his model with measurements show good accuracy for geometries with infinite edges[2–4] and Ouis has applied Biot–Tolstoy's model in room acoustics to studies of a room with balconies, a case which can be modeled with infinite edges.[5]

An earlier alternative to the Biot–Tolstoy solution has been the Kirchhoff diffraction approximation, which can be used for both frequency- and time-domain methods. In seismics,[6,7] as well as in room acoustics,[8] the Kirchhoff diffraction approximation has commonly been employed in time-domain methods for edge diffraction. However, as has been shown using the Biot–Tolstoy expressions,[9] and other accurate methods,[10] the Kirchhoff diffraction approximation leads to large errors, not only for low frequencies but also for high frequencies in certain directions. Consequently, the Biot–Tolstoy is the preferred method for impulse response models of edge diffraction.

The Biot–Tolstoy expressions, explicit as they are, do not immediately suggest how the infinite wedge expressions can be interpreted to lead to expressions for finite wedges or for multiple diffraction. Medwin, Childs, and Jebsen suggest an interpretation, ''a discrete Huygens interpretation,'' which can be used for finite wedges and also be extended to handle multiple diffraction.[3] This is the basis for numerical methods such as the wedge assemblage (WA) method.[11] Measurements of noise barriers with a finite thickness and comparisons with other calculation methods seem to support that model. Whereas Medwin's interpretation leads to numerical calculation methods, the current paper proposes an approach in which directivity functions for the secondary edge sources *á la* Medwin are derived analytically from the IR solution for the infinite wedge. The expressions for analytical directivities are directly applicable to nonstraight edges and multiple diffraction. It will be shown that these analytical expressions support Medwin's assumption for modeling first-order diffraction, namely that the contributions from the two sides of the edge around the apex point are exactly identical. On the other hand, the analytical functions indicate approximations in Medwin's assumptions for second- and higher-order diffraction. These approximations, however, seem to be of minor importance for geometries

[a]Present address: Department of Telecommunications, Norwegian University of Science and Technology, N-7491 Trondheim, Norway.
[b]Present address: Akustik Forum AB, Stampgatan 15, SE-416 64 Göteborg, Sweden.

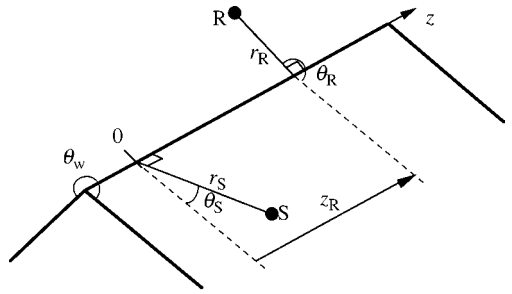

FIG. 1. The geometry of an infinite wedge irradiated by a point source *S*. Cylindrical coordinates are used with the *z*-axis along the edge of the wedge. The source has coordinates r_S and θ_S and is placed at $z_S=0$. The receiver has the coordinates r_R, θ_R, and z_R and the wedge has an open angle of θ_w.

where the second-order sound paths pass edges with small angle deviations, as in most noise-barrier cases.

Section I of this paper reviews the Biot–Tolstoy solution and Medwin's extension to this. A new derivation using analytical directivity functions is presented, and its extension to second-order diffraction is described. In Sec. II the numerical calculation of edge diffraction impulse responses is discussed. Section III presents numerical calculations for finite edges and analytical derivations for a thin circular disc. The wealth of exact and asymptotic frequency-domain solutions (see Pierce[12] for a review) is addressed here only for comparisons with calculations where the uniform theory of diffraction (UTD) by Kouyoumjian and Pathak is used.[13]

I. THEORY

The problem to be considered here is that of a point source irradiating a rigid or soft, (i.e., pressure-release) object, a special case of which is the infinite wedge. Impulse responses will be used throughout as descriptors of the sound fields, with the sound pressure $p(t)$ as output signal and a source signal $q(t)=\rho_0 A(t)/(4\pi)$, where ρ_0 is the density of the air and $A(t)$ the volume acceleration of the point source. Free-field radiation is then described by the IR, $h_{\mathrm{FF}}(\tau)=\delta(\tau-R/c)/R$, where R is the source-to-receiver distance. The IR for plane-surfaced objects can be written as a sum of the geometrical acoustics IR, h_{GA}, and diffraction components h_{diffr}. The direct sound and specular reflections of first and higher orders will be contained in h_{GA}, as long as their respective validity criteria are fulfilled. In the case of an object with an entirely convex geometry (i.e., no indents), h_{diffr} will consist of only first- and higher-order edge diffraction, whereas other geometries might cause combinations of specular reflections and edge diffraction. In this study, only convex geometries will be considered, in particular infinite and finite wedges, and circular and rectangular plates.

As a starting point, consider an infinite rigid wedge with a geometry as indicated in Fig. 1 where the cylindrical coordinates r_S, θ_S, 0 are used for the source and r_R, θ_R, z_R for the receiver. The edge diffraction IR can be written in a form which is a combination of the forms given in Refs. 3 and 14, and based on the solution presented in Ref. 1,

$$h_{\mathrm{diffr}}(\tau)=-\frac{c\nu}{2\pi}\frac{\beta(\tau)}{r_S r_R \sinh\eta(\tau)}H(\tau-\tau_0), \tag{1}$$

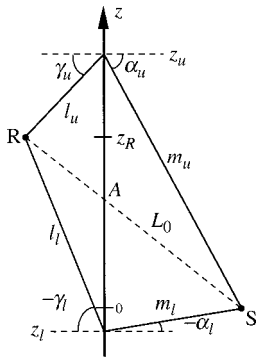

FIG. 2. A plane view of the edge constructed from the two half-planes containing the edge and the source *S*, and the edge and the receiver *R*, respectively. Two *z*-coordinates, z_l and z_u, are indicated for which the two sound paths $S-z_l-R$ and $S-z_u-R$ have identical path lengths. Also indicated is the shortest distance, L_0, via the apex point, denoted *A*, of the edge. Angles are defined with signs so that $\sin\alpha=z/m$ and $\sin\gamma=(z-z_R)/l$.

where

$$\beta(\tau)=\beta_{++}(\tau)+\beta_{+-}(\tau)+\beta_{-+}(\tau)+\beta_{--}(\tau), \tag{2}$$

$$\beta_{\pm\pm}(\tau)=\frac{\sin[\nu(\pi\pm\theta_S\pm\theta_R)]}{\cosh[\nu\,\eta(\tau)]-\cos[\nu(\pi\pm\theta_S\pm\theta_R)]}, \tag{3}$$

$$\eta(\tau)=\cosh^{-1}\frac{c^2\tau^2-(r_S^2+r_R^2+z_R^2)}{2r_S r_R}, \tag{4}$$

where c is the speed of sound, the wedge index ν equals π/θ_w, $H(\tau-\tau_0)$ in Eq. (1) is Heaviside's unit step function, and the time τ_0 equals L_0/c. The distance $L_0=[(r_S+r_R)^2+z_R^2]^{1/2}$ is the shortest path from the source to the receiver via the edge of the wedge, passing through the so-called apex point of the edge, indicated as A in Fig. 2. For an infinite wedge with soft (pressure-release) surfaces, the IR is given by using a modified version of the β-expression[15]

$$\beta_{\mathrm{soft}}(\tau)=-\beta_{++}(\tau)+\beta_{+-}(\tau)+\beta_{-+}(\tau)-\beta_{--}(\tau). \tag{5}$$

Wedges with a combination of rigid and soft surfaces could be studied using variants of the β-expressions in Eqs. (2) or (5); however, in the following discussion, rigid surfaces will always be assumed except for the example of a circular soft disc, studied in Sec. III B.

A. Models of finite wedge diffraction

Although the analytical solution in Eq. (1) describes explicitly the IR of an infinite wedge, it does not indicate what a solution for a finite wedge might look like. Medwin *et al.* suggest a ''discrete Huygens interpretation,''[3] placing a number of small secondary sources along the edge and adjusting their strengths so that together they give the known exact solution. According to this model, these secondary sources emit pulses when they are hit by the incident, impulsive, sound wave. Thus, the reaction at the edge is assumed to be instantaneous. This leads to the conclusion that the value of the IR h_{diffr} at time τ is caused by the reradiation from the two parts of the edge indicated in Fig. 2, a lower

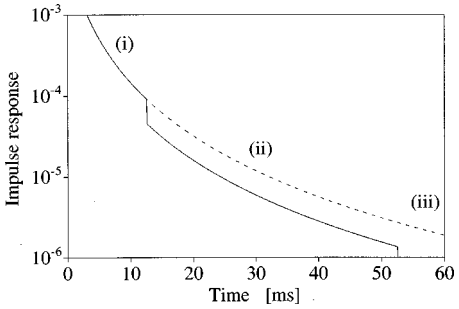

FIG. 3. Illustration of a diffraction impulse response for a finite wedge, h_{finite} (solid line) and the corresponding infinite wedge, h_{infinite} (dotted line), indicating the three parts where [i] $h_{\text{finite}}=h_{\text{infinite}}$, [ii] h_{finite} is a scaled version of h_{infinite}, and [iii] where $h_{\text{finite}}=0$. The initial part of the impulse responses has been truncated.

branch indicated by the subscript l, and an upper branch indicated by a subscript u. The two branches must obey the condition

$$m_l + l_l = m_u + l_u = c\tau. \tag{6}$$

The two edge portions at positions z_l and z_u will cause two radiated sound-field components, h_l and h_u, which summed together equal the known amplitude h_{diffr},

$$h_l(\tau) + h_u(\tau) = h_{\text{diffr}}(\tau). \tag{7}$$

As indicated in Fig. 3, an IR for a single finite wedge will then have three parts. In the initial part, [i], the IR is identical to the infinite wedge response. In the final part, [iii], the IR is zero, after the sound wave has reached the furthest end of the edge. The intermediate part, [ii], where only h_l or h_u in Eq. (7) is present, is then a scaled version of the infinite wedge IR. The scaling for the intermediate part was suggested in Ref. 2, and is based on the finite wedge IR having half the amplitude of the infinite wedge IR, i.e., $h_l = h_u$. In a later paper,[3] it was instead suggested that this factor should be

$$\frac{h_{\text{finite}}(\tau)}{h_{\text{infinite}}(\tau)} = \frac{h_l(\tau)}{h_l(\tau)+h_u(\tau)} = \frac{m_u l_u}{m_u l_u + m_l l_l}, \tag{8}$$

where it is assumed that the lower branch of the edge has the longest extension. It will be shown below that a theoretical derivation supports the relation $h_l = h_u$.

For multiple scattering, Medwin's model and the WA method assume that the secondary edge sources radiate as point sources, with source strength modifications based on Eq. (8). Second-order diffraction is then calculated by having all these secondary edge sources along the first edge generate individual diffraction contributions via the second edge.

Medwin *et al.* present comparisons between measurements and calculations for noise barriers of finite widths where second-order diffraction must be taken into account, and the agreement seems to be quite good.[3] The agreement is also good for the scattering from a circular disc.[11] As will be shown in Sec. I C, however, the derived analytical directivity functions indicate that having the secondary sources along the first edge use the ordinary diffraction expression to generate second-order diffraction via the second edge, as in Eq. (1), is only an approximation as far as we can determine. However, the errors in Medwin's model do not appear to show up for geometries with symmetrical situations, such as for noise barriers with parallel edges. The second-order diffraction paths which will be of highest amplitude are those passing the apex points, that is, with as little angular deviation as possible during the passage of the edge. The methods in Refs. 2, 3, and 11 correctly predict these high-amplitude parts, and thus predict the second-order diffraction quite well, as long as the geometry is such that sound paths with little angular deviation are possible. A critical benchmark case would then be one where all sound paths across edges experience large angular deviation. For such cases, an accurate secondary source model would be important.

B. Derivation of analytical directivity functions for the secondary edge source

A derivation of analytical directivity function for the secondary edge sources starts by assuming the existence of a directivity function for the secondary edge sources which depends only on the angles of the incident sound path, α and θ_s, and of the reradiated sound path, γ and θ_r in Figs. 1 and 2. This directivity function must be independent of the distances m and l, and must be symmetric so that the source and receiver positions can be interchanged with identical results. Thus, the reciprocity principle is always fulfilled. A consequence of such directivity functions is that the incident wavefront is split up when it hits a point of the edge, and the reradiated wavefront spreads in all directions with different amplitudes. To derive such a directivity function, the method of retarded potentials is employed as in Ref. 7, and a prototype solution can be formulated for the edge diffraction. The prototype solution is then matched to the known solution for the infinite wedge. Thus, the diffracted pressure $p_{\text{diffr}}(t)$ could be written as an integral over contributions from the entire wedge

$$P_{\text{diffr}}(t) = \int_{-\infty}^{\infty} q\left[t - \frac{m(z)+l(z)}{c}\right] \frac{D[\alpha(z),\gamma(z),\theta_S,\theta_R]}{m(z)l(z)}\,dz, \tag{9}$$

where $D[\alpha(z),\gamma(z),\theta_S,\theta_R]$ is the unknown directivity function. The position along the wedge is given by the z-coordinate, and this causes a retardation of the source signal $q(t)$, an amplitude attenuation caused by the ray paths m and l, and a further amplitude attenuation by the directivity function D. The variable z can be substituted for a variable $\tau=(m+l)/c$, the time delay. There will, however, be two values of z giving the same value of τ, corresponding to the upper and lower branches of the edge. Thus, the integral in Eq. (9) is first rewritten as a sum of the upper and lower branch integrals, as

$$p_{\text{diffr}}(t) = \int_{-\infty}^{z_{\text{apex}}} q\left[t - \frac{m(z)+l(z)}{c}\right] \frac{D[\alpha(z),\gamma(z),\theta_S,\theta_R]}{m(z)l(z)}\,dz + \int_{z_{\text{apex}}}^{\infty} q\left[t - \frac{m(z)+l(z)}{c}\right] \frac{D[\alpha(z),\gamma(z),\theta_S,\theta_R]}{m(z)l(z)}\,dz, \tag{10}$$

where z_{apex} corresponds to the apex point on the edge, which is given by $z_{\text{apex}}=z_R r_S/(r_S+r_R)$. Now, a variable substitution is carried out so that

$$p_{\text{diffr}}(t)=\int_{\infty}^{\tau_0} q(t-\tau)\frac{D_l(\tau)}{m_l(\tau)l_l(\tau)}\frac{dz_l}{d\tau}d\tau + \int_{\tau_0}^{\infty} q(t-\tau)\frac{D_u(\tau)}{m_u(\tau)l_u(\tau)}\frac{dz_u}{d\tau}d\tau = \int_{\tau_0}^{\infty} q(t-\tau)\left\{-\frac{D_l(\tau)}{m_l(\tau)l_l(\tau)}\frac{dz_l}{d\tau} + \frac{D_u(\tau)}{m_u(\tau)l_u(\tau)}\frac{dz_u}{d\tau}\right\}d\tau, \quad (11)$$

where the subscripts l and u, respectively, indicate that for each value of τ, the solution of $D(\tau)$, $m(\tau)$, $l(\tau)$, and $z(\tau)$ is chosen to correspond to the lower and upper branches, respectively. Also, in Eq. (11) the directivity function is written as $D_l(\tau)$ rather than $D[\alpha_l(\tau),\gamma_l(\tau),\theta_S,\theta_R]$. The quantities $dz/d\tau$ can then be defined as being zero before $\tau=\tau_0$, the first arrival time of the diffracted sound-field component, so that the lower integration limit can be expanded to $-\infty$. From this it becomes clear that the integral in Eq. (11) is a convolution integral of the source signal $q(t)$ with an IR which must be the diffraction IR, since

$$p_{\text{diffr}}(t)=\int_{-\infty}^{\infty} q(t-\tau)h_{\text{diffr}}(\tau)d\tau, \quad (12)$$

and $h_{\text{diffr}}(\tau)$ can be identified as

$$h_{\text{diffr}}(\tau)=-\frac{D_l(\tau)}{m_l(\tau)l_l(\tau)}\frac{dz_l}{d\tau}+\frac{D_u(\tau)}{m_u(\tau)l_u(\tau)}\frac{dz_u}{d\tau}. \quad (13)$$

To find a directivity function D which satisfies Eq. (13), the observations

$$-\frac{1}{m_l(\tau)l_l(\tau)}\frac{dz_l}{d\tau}=\frac{1}{m_u(\tau)l_u(\tau)}\frac{dz_u}{d\tau}=\frac{cH(\tau-\tau_0)}{r_S r_R\sinh\eta(\tau)}, \quad (14)$$

which are proven in Appendix A, will be used. The relations in Eq. (14) can be inserted into Eq. (13), which leads to

$$-\frac{v\beta(\tau)}{2\pi}=D[\alpha_l(\tau),\gamma_l(\tau),\theta_S,\theta_R] + D[\alpha_u(\tau),\gamma_u(\tau),\theta_S,\theta_R]. \quad (15)$$

Furthermore, it is possible to express β as function of the angles α and γ. To do this, another relation shown in Appendix B,

$$\eta(\tau)=\cosh^{-1}\frac{1+\sin\alpha(\tau)\sin\gamma(\tau)}{\cos\alpha(\tau)\cos\gamma(\tau)}, \quad (16)$$

can be used. It should be noted that α and γ can be exchanged without affecting the result, and thus reciprocity is assured. This relation is valid regardless of whether one chooses the lower or upper branch combination of the α and γ angles, an observation which could be formulated as $\eta[\alpha_l(\tau),\gamma_l(\tau),\theta_S,\theta_R]=\eta[\alpha_u(\tau),\gamma_u(\tau),\theta_S,\theta_R]$ and consequently, $\beta[\alpha_l(\tau),\gamma_l(\tau),\theta_S,\theta_R]=\beta[\alpha_u(\tau),\gamma_u(\tau),\theta_S,\theta_R]$, so it can be stated that

$$\beta(\tau)=\tfrac{1}{2}\{\beta[\alpha_l(\tau),\gamma_l(\tau),\theta_S,\theta_R] + \beta[\alpha_u(\tau),\gamma_u(\tau),\theta_S,\theta_R]\}. \quad (17)$$

This expression can finally be inserted into Eq. (15), and the unknown directivity function D can be identified as

$$D[\alpha(\tau),\gamma(\tau),\theta_S,\theta_R]=-\frac{v\beta[\alpha(\tau),\gamma(\tau),\theta_S,\theta_R]}{4\pi}, \quad (18)$$

where either $\alpha_l(\tau)$ and $\gamma_l(\tau)$, or $\alpha_u(\tau)$ and $\gamma_u(\tau)$, could be chosen as solutions for $\alpha(\tau)$ and $\gamma(\tau)$. These derivations lead to the conclusion that the branches of the edge on each side of the apex point contribute with exactly equal amounts to the diffraction IR $h_{\text{diffr}}(\tau)$. This has two consequences. First, one could choose either the upper or lower branch solutions for $\alpha(\tau)$, $\gamma(\tau)$, $z(\tau)$, $m(\tau)$, and $l(\tau)$ to formulate the total diffraction IR in this new form,

$$h_{\text{diffr}}(\tau)=-\frac{v}{4\pi}\frac{\beta[\alpha(\tau),\gamma(\tau),\theta_S,\theta_R]}{m(\tau)l(\tau)}\frac{dz}{d\tau}, \quad (19)$$

where β is as in Eqs. (2) and (3), and uses $\eta(\tau)$ from Eq. (16). Second, for a finite wedge, $h_l(t)=h_u(t)$ in Eq. (7), i.e., the part of the IR which is a scaled version of the infinite wedge IR, illustrated as part [ii] in Fig. 3, has the simple scaling factor 1/2,

$$\frac{h_{\text{finite}}(\tau)}{h_{\text{infinite}}(\tau)}=\frac{1}{2}. \quad (20)$$

This scaling factor supports the suggestion by Medwin in Ref. 2, but contradicts the suggested relationship in Ref. 3, as discussed in Sec. I A.

Decomposition of the infinite wedge diffraction into local edge contributions also makes it possible to derive diffraction from nonstraight edges. As is shown below among the examples in Sec. III, the first- and second-order diffraction components of a circular thin disc can be derived analytically. Such derivations can employ a rewritten version of the original expression in Eq. (9), using the β function, as

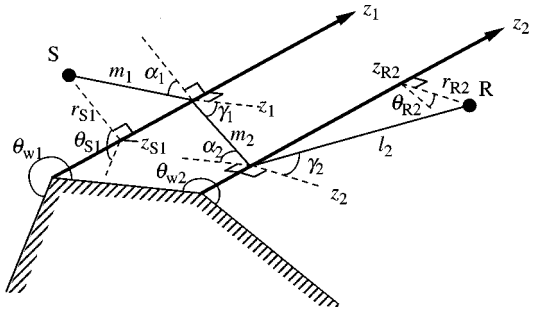

FIG. 4. The geometry of a truncated infinite wedge, with two parallel infinite edges, a point source S and a receiver R. One sound path, via the two points z_1 and z_2 on the two edges, is marked. For the first edge with the open wedge angle θ_{w1}, the source S has the cylindrical coordinates r_{S1}, θ_{S1}, z_{S1}, and the point at z_2 along edge 2, which acts as a receiver, has the coordinates w,θ_{w1},z_2. Relative to the second edge with the open wedge angle θ_{w2}, the point z_1 along edge 1 acts as a source and has the coordinates w, $\theta_{S2}=0$, z_1, and the receiver R has the coordinates r_{R2}, $\theta_{w2}-\theta_{R2}$, z_{R2}. It is assumed that the two z-axes are aligned with respect to each other. The angles α and γ are as defined in Fig. 2.

$$p_{\text{diffr}}(t) = -\frac{v}{4\pi}\int_{z_1}^{z_2} q\left[t - \frac{m(z)+l(z)}{c}\right] \times \frac{\beta[\alpha(z),\gamma(z),\theta_S,\theta_R]}{m(z)l(z)}\,dz, \tag{21}$$

where z_1 and z_2 are the two endpoints of the finite or infinite wedge.

C. Second-order edge diffraction

To derive expressions for second-order diffraction, the case of a truncated infinite wedge with two parallel, infinitely long edges as in Fig. 4 is studied. Expanding the formulation in Eq. (21), and using the sound-path designations in Fig. 4, the second-order diffracted pressure can be written

$$p_{\text{diffr}}(t) = \frac{v_1 v_2}{(4\pi)^2}\int\int_{-\infty}^{\infty} q\left[t - \frac{m_1(z_1)+m_2(z_1,z_2)+l_2(z_2)}{c}\right] \frac{\beta[\alpha_1(z_1),\gamma_1(z_1,z_2),\theta_{S1},0]\beta[\alpha_2(z_1,z_2),\gamma_2(z_2),0,\theta_{R2}]}{2m_1(z_1)m_2(z_1,z_2)l_2(z_2)}\,dz_1 dz_2, \tag{22}$$

where it has been assumed that the path from edge 1 to edge 2 runs along a plane connecting the two edges. This is indicated by the values $\theta_{R1}=0$ and $\theta_{S2}=0$ in the two β factors and the factor of 2 in the denominator of the integral. This factor of 2 compensates for the doubling in pressure generated by an acoustic source when it is mounted on a baffle. It should have the value of 1 if the ray from edge 1 to edge 2 does not run along a plane. In the double integral in Eq. (22), the factor m_1 and the delay corresponding to m_1 can be moved out from the integral over dz_2, so that

$$p_{\text{diffr}}(t) = \frac{v_1}{4\pi}\int_{-\infty}^{\infty}\left[\frac{\delta(t-m_1(z_1)/c)}{m_1(z_1)} * I_2\right] dz_1, \tag{23}$$

where* indicates a convolution and

$$I_2 = \frac{1}{2}\frac{v_2}{4\pi}\int_{-\infty}^{\infty} q\left[t - \frac{m_2(z_1,z_2)+l_2(z_2)}{c}\right] \frac{\beta[\alpha_1(z_1),\gamma_1(z_1,z_2),\theta_{S1},0]\beta[\alpha_2(z_1,z_2),\gamma_2(z_2),0,\theta_{R2}]}{m_2(z_1,z_2)l_2(z_2)}\,dz_2. \tag{24}$$

For each value of z_1, there is a $z_{2,\text{apex}}$ around which the integral I_2 can be split into the upper and lower branches, as was described before. Then, a variable substitution is possible with $(m_2+l_2)/c=\tau$, and the factors $dz_2/d\tau$ can be defined as being zero before $\tau=\tau_{02}$. Here, $\tau_{02}=L_{02}/c$ where $L_{02}=[(w+r_{R2})^2+(z_{R2}-z_1)^2]^{1/2}$. Since the geometry is basically the same as for the diffraction for a single wedge, the left-hand relation in Eq. (14) holds here, too. The integral I_2 can then be written

$$I_2 = \frac{1}{2}\frac{v_2}{4\pi}\int_{-\infty}^{\infty} q(t-\tau)\frac{(\beta_{1l}\beta_{2l}+\beta_{1u}\beta_{2u})}{m_2 l_2}\frac{dz_2}{d\tau}\,d\tau = q(t) * h_{\text{diffr},z_1\to R}(\tau), \tag{25}$$

where the values of m_2, l_2, and $dz_2/d\tau$ can be chosen as the upper or lower branch solutions for a certain value of τ. If one studies the impulse response $h_{\text{diffr},z_1\to R}(\tau)$ further,

$$h_{\text{diffr},z_1\to R}(\tau) = \frac{1}{2}\frac{v_2}{4\pi}\frac{1}{m_2 l_2}\frac{dz_2}{d\tau}\{\beta[\alpha_1,\gamma_{1l},\theta_{S1},0] \times \beta[\alpha_{2l},\gamma_{2l},0,\theta_{R2}] + \beta[\alpha_1,\gamma_{1u},\theta_{S1},0]\beta[\alpha_{2u},\gamma_{2u},0,\theta_{R2}]\}. \tag{26}$$

Equation (17) can be applied, implying that $\beta[\alpha_{2l},\gamma_{2l},0,\theta_{R2}]=\beta[\alpha_{2u},\gamma_{2u},0,\theta_{R2}]$ and

$$h_{\text{diffr},z_1\to R}(\tau) = \frac{1}{2}\frac{v_2}{4\pi}\frac{\beta(\alpha_{2u},\gamma_{2u},0,\theta_{R2})}{m_2 l_2}\frac{dz_2}{d\tau} \times \{\beta[\alpha_1,\gamma_{1l},\theta_{S1},0]+\beta[\alpha_1,\gamma_{1u},\beta_{S1},0]\} = h_{\text{diffr,1st,edge2}}(\tau)\{\beta[\alpha_1,\gamma_{1l},\theta_{S1},0] + \beta[\alpha_1,\gamma_{1u},\theta_{S1},0]\}/2. \tag{27}$$

This means that the IR $h_{\text{diffr},z_1\to R}(\tau)$ is a first-order edge-diffraction IR from the position z_1 on edge 1 to the receiver position R via edge 2, scaled by 1/2, and multiplied with a weighting function which is the sum of the two β functions in Eq. (27). The approach for second-order diffraction in Ref. 3 is to place discrete edge sources along edge 1, and to use an ordinary first-order diffraction IR to calculate their contributions at the receiver point. However, the factor with two β functions in Eq. (27) will modify the first-order diffraction IR $h_{\text{diffr,1st,edge2}}$, which in principle makes it impossible to let the edge sources on edge 1 irradiate edge 2 via ordinary first-order diffraction IRs. The method used in Ref. 3 probably does calculate the onset of $h_{\text{diffr},z_1\to R}(\tau)$ correctly and, since the high-frequency properties are determined to a large degree by the transient onset, the overall second-order edge diffraction is predicted rather well. Employing the IR $h_{\text{diffr},z_1\to R}$, the second-order diffracted pressure becomes

$$p_{\mathrm{diffr}}(t)$$
$$= \frac{v_1}{4\pi}\int_{-\infty}^{\infty}\left\{\frac{\delta[t-m_1(z_1)/c]}{m_1(z_1)} * [q(t) * h_{\mathrm{diffr},z_1\to R}(z_1,t)]\right\} \times dz_1$$
$$= q(t) * \left\{\frac{v_1}{4\pi}\int_{-\infty}^{\infty}\left[\frac{\delta[t-m_1(z_1)/c]}{m_1(z_1)} * h_{\mathrm{diffr},z_1\to R}(z_1,t)\right] \times dz_1\right\}. \quad (28)$$

This expression means that the second-order diffraction IR, $h_{\mathrm{diffr,2nd}}(\tau)$, can be found from a single integral,

$$h_{\mathrm{diffr,2nd}}(\tau)$$
$$= \frac{v_1}{4\pi}\int_{-\infty}^{\infty}\left[\frac{\delta[\tau-m_1(z_1)/c]}{m_1(z_1)} * h_{\mathrm{diffr},z_1\to R}(z_1,\tau)\right] dz_1$$
$$= \frac{v_1}{4\pi}\int_{-\infty}^{\infty}\frac{h_{\mathrm{diffr},z_1\to R}[\tau-m_1(z_1)/c]}{m_1(z_1)}\,dz_1. \quad (29)$$

However, since the IR $h_{\mathrm{diffr},z_1\to R}(\tau)$ is zero for $\tau<\tau_{02}$, the infinite integration limits in Eq. (29) can be replaced by the values $z_{1,1}$ and $z_{1,2}$, which both satisfy $\tau=\tau_{02}+m_1/c$. Explicit solutions to Eq. (29) might be possible for certain geometries, for instance the axisymmetric reflection from a circular disc, as shown in Sec. III B.

II. NUMERICAL IMPLEMENTATION—DISCRETE-TIME IMPULSE RESPONSES

The default solution for numerical calculations is to use a discrete-time IR which, for instance, can be given by area sampling of the continuous-time expression in Eqs. (1) or (19). A value of the discrete-time diffraction IR $h_{\mathrm{diffr}}(n)$ at a certain discrete time $\tau=n/f_s$, where f_s is the sampling frequency and n is a sample number, is thus given by

$$h_{\mathrm{diffr}}(n)=\int_{(n-1/2)/f_s}^{(n+1/2)/f_s} h_{\mathrm{diffr}}(\tau)\,d\tau, \quad (30)$$

where $h_{\mathrm{diffr}}(\tau)$ is the continuous-time diffraction IR, such as in Eq. (1). The singularity at $\tau=\tau_0$ in Eq. (1) deserves special attention, and the original function can be approximated by an analytically integrable function for values of τ close to τ_0.[14] The integration in Eq. (30) corresponds to filtering the continuous-time signal $h_{\mathrm{diffr}}(\tau)$ prior to sampling, employing a low-pass filter with an IR in the form of a rectangular pulse of width $1/f_s$. This is quite a crude low-pass filter, and Clay and Kinney suggest the use of a wider pulse of width $4/f_s$.[14] The sampling frequency can, however, always be raised high enough to give a low enough aliasing error at the highest frequency of interest. In the numerical examples in this study, numerical integration as in Eq. (30) has been used throughout with rather high sampling frequencies (20 to 40 times the highest frequency of interest) to get accurate results.

Formulating the diffraction as a sum of contributions from along the edge, as in Eq. (19), it can be seen that the integration of $h_{\mathrm{diffr}}(\tau)$ in Eq. (30) over a time segment $d\tau$ is equivalent to the integration over a segment of the edge which corresponds to this particular $d\tau$. To do this, another variable substitution can be done so that

$$h(n)=\int_{(n-0.5)/f_s}^{(n+0.5)/f_s} h_{\mathrm{diffr}}(\tau)\,d\tau=\int_{z_{n1}}^{z_{n2}} h_{\mathrm{diffr}}(z)\frac{d\tau}{dz}\,dz, \quad (31)$$

where z_{n1} and z_{n2} are the z-coordinates that correspond to $\tau=(n\pm1)/(2f_s)$, respectively. As discussed in conjunction with Eq. (19), one could choose either the lower or upper branch z-coordinates that correspond to τ. Since Eq. (19) can be used to find that

$$h_{\mathrm{diffr}}(z)\frac{d\tau}{dz}=-\frac{v}{4\pi}\frac{\beta[\alpha(z),\gamma(z),\theta_S,\theta_R]}{m(z)l(z)}, \quad (32)$$

the integration in Eq. (31) can be written

$$h(n)=-\frac{v}{4\pi}\int_{z_{n1}}^{z_{n2}}\frac{\beta[\alpha(z),\gamma(z),\theta_S,\theta_R]}{m(z)l(z)}\,dz. \quad (33)$$

This integration can be approximated by the midpoint value so that

$$h(n)\approx-\frac{v}{4\pi}\frac{\beta[\alpha(z_n),\gamma(z_n),\theta_S,\theta_R]}{m(z_n)l(z_n)}\Delta z_n, \quad (34)$$

where z_n is the midpoint between z_{n1} and z_{n2}. If, for a simplified numerical implementation, one chooses to divide the edge into equally sized elements of size Δz, then an element i placed at z_i will give a contribution Δh_i to the IR

$$\Delta h_i\approx-\frac{v}{4\pi}\frac{\beta[\alpha(z_i),\gamma(z_i),\theta_S,\theta_R]}{m(z_i)l(z_i)}\Delta z. \quad (35)$$

This should be added to a single time sample $n=f_s(m+l)/c$ or divided among two or more consecutive time samples. This division is determined by the edge element's position and size relative to the time positions for sample n. The contribution Δh_i should be viewed as a rectangular pulse with a width Δt as given by the element size Δz and its position z_i. If the edge element size is chosen so that $\Delta z<c/f_s$, the contribution from each element will never spread out over more than two time samples.

For efficient numerical implementations, the β function can be written in a much more compact form than in Eqs. (2), (3), and (16) if one uses the relation

$$\cosh(v\eta)=(A^v+A^{-v})/2, \quad (36)$$

where $A=(y^2-1)^{1/2}+y$ and $y=[ml+z(z-z_r)]/(r_s r_r)$, which is taken from Eq. (A7), with the same variables as before. With this formulation, only basic mathematical computations need to be recalculated for each edge element and very efficient implementations are possible.

Second-order diffraction is straightforward to implement using a formulation which is based on Eq. (22). If two finite edges are divided into equally sized edge elements Δz_1 and Δz_2, the second-order contribution Δh_{ij} to the IR $h_{\mathrm{diffr,2nd}}$, of edge element i at z_i of edge 1 and edge element j at z_j of edge 2, can be written

$$\Delta h_{ij}=\frac{v_1 v_2}{32\pi^2}\frac{\beta[\alpha_1(z_1),\gamma_1(z_1,z_2),\theta_{S1},\theta_{R1}]\beta[\alpha_2(z_1,z_2),\gamma_2(z_2),\theta_{S2},\theta_{R2}]}{m_1(z_1)m_2(z_1,z_2)l_2(z_2)}\Delta z_1,\Delta z_2. \tag{37}$$

This expression is valid for both parallel and nonparallel edges, as long as the appropriate expressions for the involved α, γ, and θ angles, and m and l distances, are used. Note that a second-order contribution via two edge elements should be viewed as a triangular pulse, and a third-order contribution appears as a pulse with second-order polynomial shape, etc. This affects how each contribution should be divided among time samples. A simplified implementation, giving the correct low-frequency response, was used by Vanderkooy.[16] The contribution Δh can be distributed over the two time samples adjacent to the arrival time of the edge element center, with a linear weighting that depends on the center arrival time's position relative to the two sample times.

Other models have used time-domain formulations for edge diffraction, the most common ones being based on the Kirchhoff diffraction approximation, as mentioned in the Introduction. Another model, suggested by Vanderkooy, has an interesting equivalence to the new model suggested here.[16] Vanderkooy's model started from a frequency-domain high-frequency asymptotic expression for the infinite wedge.[17] The model uses discrete edge sources, each of which gives a contribution

$$\Delta h=-\frac{v}{4\pi}\frac{\kappa(\theta_S,\theta_R)}{ml}\Delta z, \tag{38}$$

which is delayed by the time $\tau=(m+l)/c$. Vanderkooy used a parameter v_{Vand} which is the reciprocal of the wedge index v used here, but for clarity the parameter v_{Vand} was replaced by v in Eq. (38) so that the similarity with Eq. (35) is clear. The directivity function κ is

$$\kappa(\theta_S,\theta_R)=\sin v\pi\left\{\frac{1}{\cos v\pi-\cos[v(\theta_R-\theta_S)]}+\frac{1}{\cos v_\pi+\cos[v(2\pi-\theta_R-\theta_S)]}\right\}, \tag{39}$$

which can be rewritten into the form

$$\kappa(\theta_S,\theta_R)=\beta_{++}^{\mathrm{Vand}}+\beta_{+-}^{\mathrm{Vand}}+\beta_{-+}^{\mathrm{Vand}}+\beta_{--}^{\mathrm{Vand}}, \tag{40}$$

where

$$\beta_{\pm\pm}^{\mathrm{Vand}}=\frac{\sin[v(\pi\pm\theta_S\pm\theta_R)]}{1-\cos[v(\pi\pm\theta_S\pm\theta_R)]}. \tag{41}$$

If $\cosh(v\eta)=1$, which happens for the time $\tau=\tau_0$ (i.e., at the onset of the diffraction), these β terms are identical with the analytical ones in Eqs. (2) and (3). Since rapid variations in the IR always occur at the onset, the high-frequency part of the response is determined entirely by this initial part of the diffracted signal. Thus, it is not surprising that Vanderkooy's model correctly reproduces the initial part of the IR and consequently the high-frequency response. The model does, however, give large errors at low frequencies, which is clearly due to using the constant value 1 in Eq. (41) instead of the monotonically increasing function $\cosh v\eta$.

III. EXAMPLES

In this section, the new model employing analytical directivity function for the secondary edge sources is compared with other methods. Only IRs have been discussed so far, but results are often more interesting when presented as transfer functions. These are calculated from the IRs using a discrete Fourier transform (DFT), and it is then possible to check if a sufficiently high sampling frequency has been used. The sampling frequency should be increased until the results at the highest frequencies of interest have stabilized. In all calculations, unless otherwise stated, a value of 344 m/s has been used for the speed of sound.

A. Infinite wedges

Two different infinite and rigid wedges were studied as illustrated in Fig. 5. Figure 5(a) shows a thin plate edge, with one fixed source position S (with cylindrical coordinates $r_S=25\,\mathrm{cm}$, $\theta_S=15°$, and $z_S=0$) and with two different receiver positions, R1 and R2 (at $r_R=25\,\mathrm{cm}$, $z_R=0$, and $\theta_R=300°$ for R1, and $\theta_R=196°$ for R2). The position R2 is 1° into the shadow zone, which is critical from a numerical point of view due to the singularity of the diffraction IR at the boundary of shadow zones. In Fig. 5(b), another case is shown with a plate of thickness w, an example which is duplicated from Ref. 3. In this case, the source is at cylindrical coordinates $r_S=25\,\mathrm{cm}$, $\theta_S=15°$, and the receiver is at $r_R=25\,\mathrm{cm}$, $\theta_R=300°$, $z_R=0$. It should be noted that because of the width w of the plate, the receiver coordinates are relative to the second edge, closest to the receiver.

Calculations of IRs were made with the new model using the discrete edge decomposition described by Eq. (35) for the single edge, and by Eq. (37) for the double edge. IRs

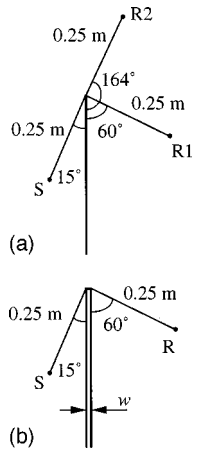

FIG. 5. The two infinite wedge situations that have been studied. (a) shows a thin plate edge. (b) shows a plate of thickness w, where the values $w=5$, 22, and 35 mm have been studied.

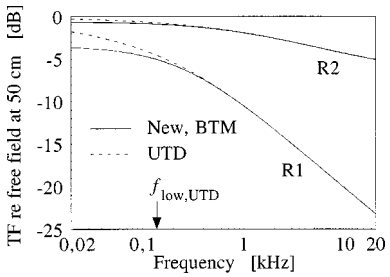

FIG. 6. Transfer function (relative to free-field propagation) at 50 cm distance for the two receiver points at the infinite wedge in Fig. 5(a). The frequency marked, $f_{low,UTD}$, is the frequency above which the UTD method should give less than 0.5 dB error according to Ref. 16.

were also calculated with the Biot–Tolstoy model from Ref. 3, here denoted BTM, and transfer functions were calculated for the single edge with the uniform theory of diffraction (UTD) by Kouyoumjian and Pathak.[13] The lowest frequency for which the UTD method gives accurate results—that is, within 0.5 dB of exact solutions—was found to be $f_{low,UTD} \approx 140$ Hz based on Fig. 4 in Ref. 18. Sampling frequencies of 800 kHz were used for the IRs since, compared with a sampling frequency of 400 kHz, the difference was less than 0.1 dB at 20 kHz. The edge element sizes were 0.43 mm for all cases, and the wedge had an extension of ± 5 m relative to the source.

Results for the wedge in Fig. 5(a) are presented in Fig. 6, where the results for the new model and the BTM model come within 0.001 dB. It can also be seen that the UTD method is indeed accurate down to $f_{low,UTD} \approx 140$ Hz. Figure 7 shows results for the double-edge wedge in Fig. 5(b), together with single-edge diffraction for the corresponding infinitely thin wedge. Comparing these results with Fig. 9 in Ref. 3, it can be seen that the results with the new method and the BTM results are very close to each other. As is also observable for the double-edge plates in Ref. 3, the differences between the thin plate limit and the low-frequency results decrease with decreasing thicknesses, yet a small but significant difference always remains. This remaining difference is probably caused by the lack of higher-order diffraction components in these calculations. It can also be noted

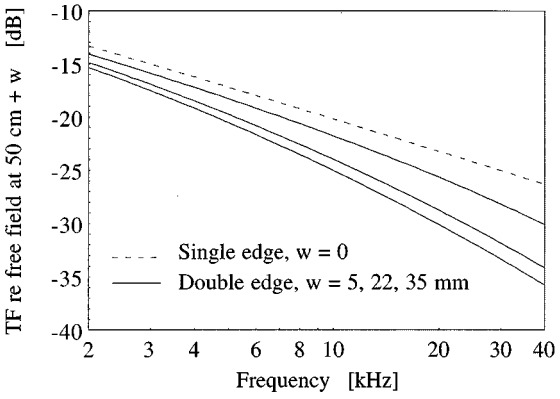

FIG. 7. Transfer function (relative to free-field propagation) at 50 cm$+w$ for the infinite plate in Fig. 5(b), calculated with the new method. The dashed line indicates the single-edge case, that is, the thin plate limit. Solid lines give results for a double wedge with $w=5$, 22, and 35 mm (from the top).

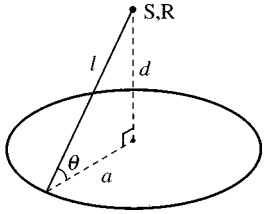

FIG. 8. The geometry for the axisymmetric scattering from a thin, rigid circular disc of radius a, with colocated source and receiver at height d.

that this new model and the BTM model give very similar results for double-edge diffraction for a geometry with parallel long edges, a happenstance that does not display well the significant differences in the two theories.

B. On-axis scattering from a rigid circular disc

The cases of on-axis scattering from rigid and soft circular discs was studied in Ref. 11, employing both an accurate, frequency-domain T-matrix formalism, and time-domain expressions using the WA method. The accurate frequency-domain expressions were transformed into IRs using the inverse discrete Fourier transform, and adjusting the sampling frequencies to the geometry so that delays corresponded to exact integer sample numbers, which should ensure that accurate time-domain expressions were retrieved. Thus, these could be seen as accurate reference cases against which the present method can be compared. Nevertheless, although the possible effects of windowing on the time signal were mentioned in Ref. 11, no estimate was given. The first-order diffraction is a single pulse, for which it should in principle be possible to accurately find the amplitude. Since second- and higher-order diffraction components are continuous-time signals with onsets exactly at the arrival of the first-order impulse, these higher-order components will inevitably influence the sample in which the impulse arrives. This effect is small since the onset amplitude of the higher-order diffraction is very small, but the accumulated effect is not clear.

To derive analytical expressions for the diffraction IR, the formulation in Eq. (21) is used. The β function must be found for the case with the source and receiver colocated, as illustrated in Fig. 8. In this case, the angles θ_S and θ_R are equal and consequently, both will be referred to as θ. The β function can be derived using the form of $\cosh(\nu\eta)$ which is valid for the wedge index $\nu=0.5$, as shown in Appendix C,

$$\cosh\frac{\eta}{2}=\frac{\cos[(\alpha-\gamma)/2]}{(\cos\alpha\cos\gamma)^{1/2}}, \tag{42}$$

which, as is also shown in Appendix C, leads to

$$\beta=2\cosh\frac{\eta}{2}\left\{\frac{\cos[(\theta_S+\theta_R)/2]}{\cosh^2(\eta/2)-\sin^2[(\theta_S+\theta_R)/2]}+\frac{\cos[(\theta_S-\theta_R)/2]}{\cosh^2(\eta/2)-\sin^2[(\theta_S-\theta_R)/2]}\right\}. \tag{43}$$

When θ_S equals θ_R and both are denoted θ, β can be written

TABLE I. Amplitude of the first-order diffraction component for axisymmetric scattering from a circular rigid disc of radius 1 m, normalized to the specular reflection. Results are either calculated using the new method, Eq. (47), or taken from Ref. 11. The errors are relative to the T-matrix solution which is considered as the reference result.

Height [m]	T matrix (Ref. 11)	WA (Ref. 11)	Rel. error [%]	Eq. (47)	Rel. error [%]
1.1	−1.221	−1.223	(−0.16)	1.238	(−1.4)
1.5	−1.273	1.247	(2.0)	−1.294	(−1.6)
3.0	−1.243	−1.252	(−0.7)	−1.249	(−0.5)
5.0	−1.163	−1.118	(3.9)	−1.173	(−0.9)
10.0	−1.093	−1.099	(−0.5)	−1.094	(−0.1)

$$\beta=\frac{2}{\cosh(\eta/2)}+\cos\theta\left[\frac{1}{\cosh(\eta/2)+\sin\theta}+\frac{1}{\cosh(\eta/2)-\sin\theta}\right]. \tag{44}$$

Furthermore, the $\cosh(\eta/2)$ factor is simplified for the axisymmetric case that is studied here. For the entire circular edge, the incident ray angles α and the reradiated ray angles γ will have the value 0, and then the quantity $\cosh(\eta/2)=1$, as is clear from Eq. (42). The β function in Eq. (44) can consequently be further simplified as

$$\beta=2+\cos\theta\left(\frac{1}{1+\sin\theta}+\frac{1}{1-\sin\theta}\right)=2\left(1+\frac{1}{\cos\theta}\right)=2\frac{a+l}{a}, \tag{45}$$

where a is the radius of the disc and $l=(a^2+d^2)^{1/2}$, d being the height of the source and receiver above the disc. Inserting this constant value of the β term into Eq. (21), together with the constant values of m and l, it is found that if the z-coordinate runs along the disc perimeter,

$$p_{\mathrm{diffr}}(t)=-\frac{a+l}{4\pi a l^2}\int_0^{2\pi a} q\left(t-\frac{2l}{c}\right)dz=-\frac{a+l}{2l^2}q\left(t-\frac{2l}{c}\right), \tag{46}$$

where it can be noted that $p_{\mathrm{diffr}}(t)$ is nothing but a scaled and delayed version of the source signal. In other words,

$$h_{\mathrm{diffr}}(\tau)=-\frac{a+l}{2l^2}\delta\left(\tau-\frac{2l}{c}\right). \tag{47}$$

The first-order diffraction for a soft disc can be found by employing the expression in Eq. (5) and repeating the derivations above, which yields

$$h_{\mathrm{diffr,soft}}(\tau)=-\frac{a-l}{2l^2}\delta\left(\tau-\frac{2l}{c}\right). \tag{48}$$

With Eqs. (47) and (48), the value of the first-order diffraction component can be calculated directly as a Dirac impulse amplitude. In Tables I and II, the values given by Eqs. (47) and (48) are, respectively, compared with corresponding values from Ref. 11, when normalized to the specular reflection for the disc, $1/(2d)$. The results, while not identical, differ at most by 2.3%, or 0.20 dB, from the reference T-matrix results. The sign of the error is always negative for the rigid disc and positive for the soft disc so that, if the second-order diffraction component contributes within the same sample as the first-order component, the error would decrease, if just marginally. The results with the WA method, as reproduced from Ref. 11, give errors of the same magnitude as those given by Eqs. (47) and (48) but with a larger spread, because of varying signs of the errors.

An explicit expression for second-order diffraction can be derived as well, and it is done here for the rigid disc only. The expression in Eq. (22) can be used if the two z-coordinates run along the disc perimeter, from $z=0$ to $z=2\pi a$, so that

$$p_{\mathrm{diffr}}(t)=2\frac{1}{(8\pi)^2}\int\int_0^{2\pi a} q\left[t-\frac{m_1+m_2(z_1,z_2)+l_2}{c}\right]\times\frac{\beta[\alpha_1,\gamma_1(z_1,z_2),\theta_{S1},0]\beta[\alpha_2(z_1,z_2),\gamma_2,0,\theta_{R2}]}{2m_1m_2(z_1,z_2)l_2}\times dz_1dz_2. \tag{49}$$

Here, the parameters m_1 and l_2 are constant and will be denoted l; θ_{S1} and θ_{R2} are identical and will be denoted θ; and α_1 and γ_2 are both equal to zero. The initial factor 2 reflects the fact that for a thin plate, there will always be identical diffraction components via the rear side of the plate which contribute to double the second-order diffraction amplitude. Furthermore, because of rotational symmetry, one of the integrations can be replaced by a factor $2\pi a$, and any fixed value of z_1 can be used in evaluating the z_2-integration. Then, with $z_1=0$,

TABLE II. Amplitude of the first-order diffraction component for axisymmetric scattering from a circular soft disc of radius 1 m, normalized to the specular reflection. Results are either calculated using the new method, Eq. (48), or taken from Ref. 11. The errors are relative to the T-matrix solution which is considered as the reference result.

Height [m]	T matrix (Ref. 11)	WA (Ref. 11)	Rel. error [%]	Eq. (48)	Rel. error [%]
1.1	0.239	0.236	(−1.3)	0.242	(1.3)
1.5	0.364	0.366	(0.5)	0.371	(1.8)
3.0	0.634	0.642	(1.3)	0.649	(2.3)
5.0	0.777	0.782	(0.6)	0.789	(1.5)
10.0	0.890	0.880	(−1.1)	0.896	(0.7)

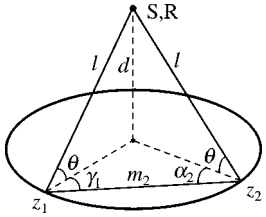

FIG. 9. Sound paths for second-order diffraction for the circular disc, indicating that the incident sound path to the first edge has a constant length l and a constant incidence angle $\alpha_1=0$. Also, the reradiated sound path from the second edge point has a constant length l and a constant angle $\gamma_2=0$. The intermediate sound path has the length m_2, and the two angles γ_1 and α_2 have the same value.

$$p_{\text{diffr}}(t)=\frac{a}{32\pi l^2}\int_0^{2\pi a} q\left[t-\frac{m_2(0,z_2)+2l}{c}\right] \times\frac{\beta[0,\gamma_1(0,z_2),\theta,0]\beta[\alpha_2(0,z_2),0,0,\theta]}{m_2(0,z_2)}dz_2. \tag{50}$$

Because of symmetry around $z_2=\pi a$, the upper integration limit can be halved, and the result doubled instead. Furthermore, a variable substitution with $(m_2+2l)/c=\tau$ leads to

$$p_{\text{diffr}}(t)=\frac{a}{16\pi l^2}\int_0^{\pi a} q(t-\tau) \times\frac{\beta[0,\gamma_1(\tau),\theta,0]\beta[\alpha_2(\tau),0,0,\theta]}{m_2(\tau)}\frac{dz_2}{d\tau}d\tau, \tag{51}$$

and, as before, the factor $dz_2/d\tau$ can be defined as being zero before $\tau=2l/c$ and after $\tau=2(l+a)/c$, so that the integration limits can be expanded to $\pm\infty$, and a convolution integral can be identified. The impulse response is then

$$h_{\text{diffr,2nd}}(\tau)=\frac{a}{16\pi l^2}\frac{\beta[0,\gamma_1(\tau),\theta,0]\beta[\alpha_2(\tau),0,0,\theta]}{m_2(\tau)}\frac{dz_2}{d\tau}. \tag{52}$$

The values of m_2, the angles γ_1 and α_2, and $dz_2/d\tau$ can be found by inspecting Fig. 9. Thus,

$$m_2=c\tau-2l, \tag{53}$$

$$\cos\gamma_1=\cos\alpha_2=\frac{m_2}{2a}, \tag{54}$$

$$z_2=a(\pi-2\gamma_1)=a\left(\pi-2\cos^{-1}\frac{m_2}{2a}\right)\Rightarrow\frac{dz_2}{d\tau}=\frac{c}{\sin\gamma_1}. \tag{55}$$

By employing the expression in Eq. (43), the product of the β functions in Eq. (52) can be molded into the form

$$\beta[0,\gamma_1(\tau),\theta,0]\beta[\alpha_2(\tau),0,0,\theta] =16\cos^2\frac{\theta}{2}\cosh^2\frac{\eta}{2}\left(\cosh^2\frac{\eta}{2}-\sin^2\frac{\theta}{2}\right)^{-2}, \tag{56}$$

where the fact that $\cosh(\eta/2)$ is identical for the two edges has been used. Using Eq. (42) and the fact that $\alpha_1=\gamma_2=0$, the function $\cosh^2(\eta/2)$ can be simplified to

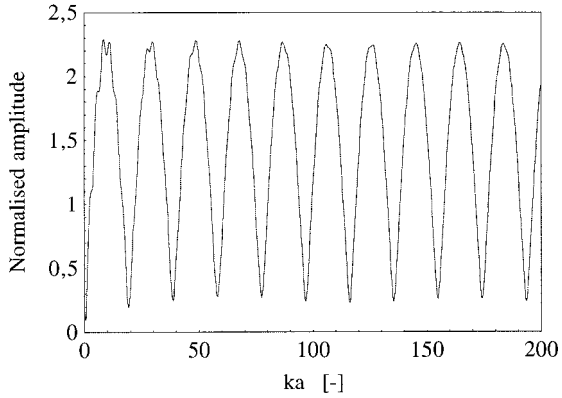

FIG. 10. Transfer function for the case in Fig. 8, with $a=1$ m and $d=3$ m, calculated with the new method. The specular reflection plus first- and second-order diffraction is included, and the amplitude is normalized to the specular reflection. The fine structure in this graph agrees with the details in Fig. 6 of Ref. 7.

$$\cosh^2\frac{\eta}{2}=\frac{1+\cos\gamma_1}{2\cos\gamma_1}, \tag{57}$$

which is valid for both the first and second edges, as $\gamma_1=\alpha_2$. If the expression in Eq. (57), together with expressions for $\sin^2(\theta/2)$ and $\cos^2(\theta/2)$, are inserted into Eq. (56), which is then used in Eq. (52), an expression for $h_{\text{diffr,2nd}}(\tau)$ results

$$h_{\text{diffr,2nd}}(\tau)=\frac{c[1+\cos\gamma_1(\tau)](1+\cos\theta)}{2\pi l^2\sin\gamma_1[1+\cos\theta\cos\gamma_1(\tau)]^2}w(\tau) =\frac{c(1+\cos\theta)}{2\pi l^2[1+\cos\theta\cos\gamma_1(\tau)]^2}\left[\frac{1+\cos\gamma_1(\tau)}{1-\cos\gamma_1(\tau)}\right]^{1/2} \times w(\tau), \tag{58}$$

where $\cos\gamma_1(\tau)$ can be found from Eqs. (53) and (54), $\cos\theta=a/l$, and $w(\tau)=H(\tau-2l/c)-H(\tau-2(a+l)/c)$. Including the first-order diffraction, Eq. (47), and second-order diffraction, Eq. (58), IRs were calculated and transformed into transfer functions. Figure 10 presents the resulting transfer function for the case with $a=1$ m and $d=3$ m. Calculation parameters were $f_s=78\,569$ Hz and a DFT size of 2048 was used. These results are very similar to those in Fig. 6 in Ref. 7. Figure 11(a) shows the second-order diffraction IR when normalized to the specular reflection amplitude $1/(2d)$.

In Ref. 11, the amplitude of the second-order diffraction was presented in terms of the peak value of the function illustrated in Fig. 11(a). This peak value is critically dependent on the sampling frequency and the low-pass filtering technique used. For purposes of comparison, the process in Ref. 11 was reproduced as closely as possible. The sampling frequency was chosen so that the delay between the specular reflection and the first-order diffraction pulse was an integer number of steps, using a speed of sound of 1500 m/s. Furthermore, an oversampling by a factor of 8 was used here and, after transforming the IR into a transfer function using a DFT size of 16 384, only the first 1024 frequencies were kept before transforming back to an IR using a DFT size of 2048.

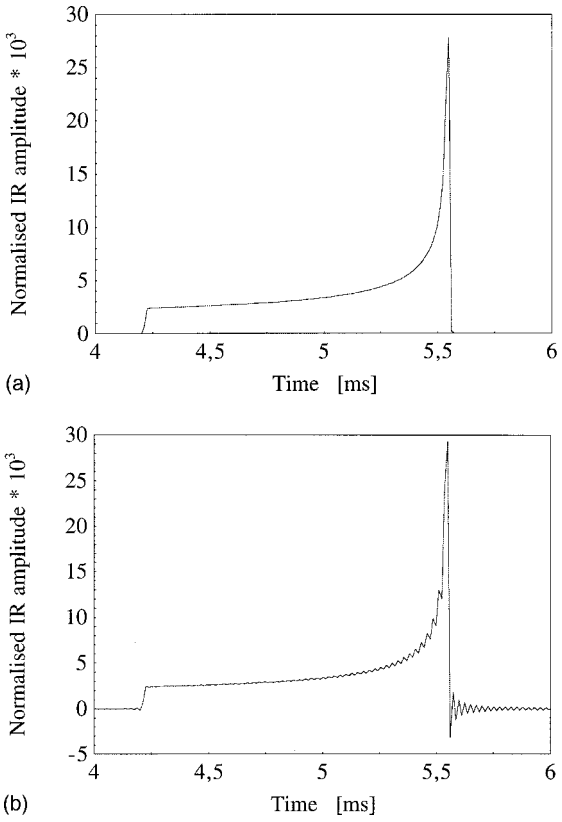

FIG. 11. Second-order diffraction impulse response for the case in Fig. 8, with $a=1$ m and $d=3$ m, calculated with the new method. The amplitude has been normalized to the specular reflection. (a) A sampling frequency of 78 569 Hz was used. (b) An oversampling by a factor of 8, relative to (a), was used and a frequency-domain low-pass filtering as described in the text gave the same final sampling frequency as in (a).

This frequency-domain low-pass filtering should be equivalent to the technique used in Ref. 11. Figure 11(b) shows an example of one such second-order diffraction IR, where the small ripple indicates the filtering effects.

Table III gives the results for the peak amplitude of the second-order diffraction IR, both when calculated using edge sources as in Eq. (50), and after the oversampling/frequency-domain filtering described above. Although the results from Ref. 11 are reproduced here, it should be noted that it is stated in Ref. 11 that the values in their Table IV are normalized to the first-order diffraction pulse rather than to the specular reflection, which is used elsewhere in that paper. We believe that this is a mistake for three reasons. First, the values in Table IV of Ref. 11 are positive rather than negative. Second, it is stated earlier in Ref. 11 that the specular reflection was used for normalization for all the results presented, even for off-axis geometries. The third argument is that our results are very close to the reference results when the specular normalization is assumed, and especially after the frequency-domain low-pass filtering was used.

The results with our new method are close enough to the reference results for the circular disc to generally support the relations derived here, but more comparisons with reference calculations should be made. Comparisons of the frequency-domain values might then be easier to carry out, avoiding ambiguities involving filtering effects as discussed above.

C. Scattering from a rectangular plate

The last example is scattering from a rectangular plate. Cox and Lam present an example of a rectangular plate of size $0.302\times1.92\times0.010$ m and with calculated directivity plots at two single frequencies, 2012 and 3995 Hz.[19] The source was positioned at a height of $d=3.96$ m, right above the center point of the plate. The receiver was moved along an arc at a constant radius of $R=1.178$ m, from the center points of the plate. The arc was in the direction of the short length of the plate. The total reflection strength was calculated using the boundary element method both for a three-dimensional model and for a thin plate limit model of the plate. It was normalized to the direct sound amplitude. Figure 12 shows results using Eqs. (35) and (37) to calculate the first- and second-order diffraction IRs for an infinitely thin model of the plate. A sampling frequency of 257 536 Hz was used, corresponding to 128 times oversampling with respect to the target frequency of 2012 Hz. The four edges were divided into 0.67-mm elements for the first-order diffraction, and twice that size for the second-order diffraction. The receiver was moved along the arc in steps of 1 deg. A DFT size of 8192 was used, to get the transfer function values exactly at 2012 Hz. The sound speed $c=346$ m/s was used in Ref. 19 and here, too.

If one compares the level of the total field in Fig. 12 with the results for the thin plate limit in Fig. 4 of Ref. 19, one can see good agreement for angles between 0 and ca. 80 deg. The larger deviations above 80 deg are probably due to the need for higher-order diffraction components. This is

TABLE III. Peak amplitude of the second-order diffraction component for axisymmetric scattering from a circular rigid disc of radius 1 m, normalized to the specular reflection. Results are either calculated using the new method [based on Eq. (50)] or taken from Ref. 11. The results denoted LPF have been low-pass filtered as described in the text. The errors are relative to the T-matrix solution which is considered as the reference results. The T matrix and WA results were specified in Ref. 11 as being relative to the first-order diffraction strength, but it has been assumed here that the specular reflection was used for the normalization as discussed in the text.

Height [m]	T matrix (Ref. 11)	WA (Ref. 11)	Rel. error [%]	Eq. (50)	Rel. error [%]	Eq. (50) (LPF)	Rel. error [%]
1.1	0.043	0.039	(−9)	0.0415	(−3)	0.0469	(+9)
1.5	0.043	0.031	(−28)	0.0374	(−13)	0.0427	(−1)
3.0	0.031	0.023	(−26)	0.0278	(−10)	0.0293	(−5)
5.0	0.024	0.016	(−33)	0.0205	(−15)	0.0234	(−3)
10.0	0.014	0.009	(−36)	0.0114	(−19)	0.0126	(−10)

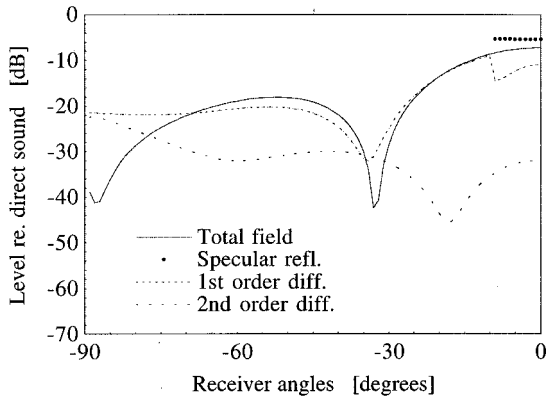

FIG. 12. Scattering from a thin rectangular plate, described in the text, calculated with the new method. Shown are levels of the total field, of the specular reflection only, of the first-order diffraction only, and of the second-order diffraction only. The frequency was 2012 Hz; the source was fixed symmetrically above the plate and the receiver position was varied along an arc.

also indicated in Fig. 12 by the large amplitude of the second-order diffraction component for large receiver angles. The deviation at the dip around 30 deg might be caused by a less dense sampling in Ref. 19, or small differences in the speed of sound. Furthermore, the smoothness of the total field around 10–12 deg, where the specular reflection disappears, indicates that the numerical method used, Eq. (35), is accurate enough up to within half a deg from the transition zone where the specular reflection disappears. This is compensated by the corresponding jump in value for the first-order diffraction. Very high oversampling was used, together with a very fine division of the edge into elements. This is needed only for the positions close to the transition zone and for the largest receiver angles. For the larger receiver angles, higher-order diffraction is needed anyway, so the total field might be calculated more accurately by using fewer edge elements but higher orders of diffraction.

A three-dimensional model of the plate was tested as well, but it was then clear that it was necessary to include higher-order diffraction since the results differed significantly from the thin plate limit model, when second-order edge diffraction was included. In conclusion, the results with the new model and the results in Ref. 19 seem to agree well enough to support the new model as long as it is realized that it may be necessary to include higher-order diffraction components for some situations.

IV. DISCUSSION AND CONCLUSIONS

The interpretation of the exact Biot–Tolstoy solution for the infinite wedge diffraction that was presented here has not been proven to be true *per se*. It has, however, been shown that if the existence of analytical directivity functions for the secondary edge sources is assumed, such functions can indeed be derived and yield the exact solution for an infinite wedge. Since this also leads to a possible application to non-straight edges, and the comparison with the result for the circular rigid disc was accurate within 0.20 dB, it is concluded that the suggested interpretation is generally valid. It should then, in principle, be possible to show that the total field, specular reflections plus diffraction components, satisfies the wave equation. The complexity of the higher-order diffraction components might, however, prevent this possibility for cases other than the infinite wedge.

The proposed model gives results that, for first-order diffraction, should be identical to those by the WA model.[11] For second-order diffraction, the results by the proposed model are very similar to results by methods which are based on Medwin's model.[3,11] Conceptually, however, the difference between Medwin's model and the proposed model is significant since the proposed model gives a complete motivation and mathematical proof for the directivity functions of the secondary edge sources.

As for the numerical implementation, very high sampling frequencies are often needed. This is because the crude low-pass ''antialiasing'' filter, which is equivalent to the single time sample integration, has a gentle roll-off characteristic. Refined integration techniques could be tested, and the directivity functions might lead to somewhat simpler functions to handle, compared to the original Biot–Tolstoy solution in Eqs. (1)–(4). Also, since each higher order of diffraction causes a response that basically falls 3 dB/octave more quickly than the previous order, lower and lower sampling frequencies could be used for each new order. This decrease occurs, however, above a cutoff frequency which is given by the size of the individual planes of the object, and the proximity to the various shadow zones. Below those frequencies, the response decreases in a way which is more difficult to predict.

Higher-order diffraction IRs should tend towards Gaussian-shaped pulses, according to the central limit theorem in statistics, since it is equivalent to convolving any function with itself many times, resulting essentially in a Gaussian function. Thus, properly time-aligned Gaussian pulses with the right areas, widths, and polarities could serve as replacement functions for higher-order diffraction.

It was shown that the case of axisymmetric backscattering from a circular disc could yield explicit expressions for the first- and second-order diffractions. It is probably possible to find such explicit expressions for several other geometries too. Further developments could lead to solutions which satisfy more general boundary conditions.

The proposed model is relevant for all cases where scattering/diffraction from idealized, rigid, or soft objects is studied, such as when the WA is applied to underwater acoustics cases, noise barriers, etc. In architectural acoustics, most IR prediction models are based on geometrical acoustics, possibly handling surface scattering, but without the possibility to handle edge diffraction accurately.[20] The Kirchhoff diffraction approximation has been tested before, but this new model should be much more accurate since it is valid at all frequencies and for all source and receiver positions.[10] In electroacoustics, edge diffraction has important applications such as the effect of the loudspeaker enclosure on the radiated sound; many simpler edge diffraction models have been tested,[16] but the proposed model should, here too, prove to be more accurate.

In conclusion, deriving analytical directivity functions for the edge sources both supports, and takes a step beyond,

previous models such as those based on Medwin's work, and gives new possibilities to solving diffraction problems in the time domain. These directivity functions support some previous first-order diffraction models, but also demonstrate that previous second-order diffraction models contain approximations, reflecting the greater accuracy of the proposed model. Derivation of explicit diffraction expressions for certain geometries, and for efficient and accurate numerical calculations, become possible using the proposed model.

ACKNOWLEDGMENTS

This project was financed in part by grants from the Swedish Institute and the Adlerbert Research Foundation, which supported the first author's research visit to the University of Waterloo. Parts of the project were also financed by the Johnson Foundation. The third author has research support from the Natural Sciences and Engineering Research Council of Canada. The authors have appreciated the comments offered by an anonymous reviewer.

APPENDIX A: PROOF OF EQ. (14)

The factor $c(r_S r_R \sinh\eta)^{-1} H(\tau-\tau_0)$ in Eq. (1) can be rewritten, introducing an auxiliary variable y,

$$\eta=\cosh^{-1} y=\log[y+(y^2-1)^{1/2}], \tag{A1}$$

so that $\sinh\eta$ can be written

$$\sinh\eta=(y^2-1)^{1/2}. \tag{A2}$$

The auxiliary variable y introduced above is [see Eq. (4)]

$$y=\frac{c^2\tau^2-(r_S^2+r_R^2+z_R^2)}{2r_S r_R}, \tag{A3}$$

and with the relation $c\tau=m+l$, y can be written

$$y=\frac{(m+l)^2-(r_S^2+r_R^2+z_R^2)}{2r_S r_R}. \tag{A4}$$

By further using the relations for m and l (see Figs. 1 and 2)

$$m=(r_S^2+z^2)^{1/2}, \tag{A5}$$

and

$$l=[r_R^2+(z-z_R)^2]^{1/2}, \tag{A6}$$

it is possible to write y as

$$y=\frac{ml+z(z-z_R)}{r_S r_R}. \tag{A7}$$

Now, using Eqs. (A2) and (A7), it can be found that

$$\begin{aligned} r_S r_R \sinh\eta &= \{[ml+z(z-z_R)]^2-r_S^2 r_R^2\}^{1/2} \\ &= [m^2l^2+z^2(z-z_R)^2+2mlz(z-z_R)-r_S^2 r_R^2]^{1/2}. \end{aligned} \tag{A8}$$

By further employing Eqs. (A5) and (A6) to get rid of r_S and r_R, it is found that

$$\begin{aligned} r_R r_R \sinh\eta &= [z^2l^2+2mlz(z-z_R)+(z-z_R)^2m^2]^{1/2} \\ &= |zl+(z-z_R)m|. \end{aligned} \tag{A9}$$

All expressions so far have been valid for both the upper and lower branch solutions of m and l. Moving temporarily to the expressions for $dz/d\tau$, this quantity can be found by studying the total path length $L=m+l$. A small increase in path length ΔL corresponds to a small increase, Δz, along the edge, and the relation between these is found by the derivative of $L(z)$

$$\frac{dL}{dz}=\frac{z}{m}+\frac{z-z_R}{l}=\frac{zl+(z-z_R)m}{ml}, \tag{A10}$$

which, using $\Delta L=c\Delta\tau$, leads to

$$\frac{1}{ml}\frac{dz}{d\tau}=\frac{c}{zl+(z-z_R)m}, \tag{A11}$$

for both the upper and lower branches of the edge, which is the left-hand relation in Eq. (14). Since $dz_u/d\tau$ is always positive, Eq. (A11) implies that $z_u l_u+(z_u-z_R)m_u$ also must always be positive. Then, Eqs. (A9) and (A11) show that the right-hand relation in Eq. (14) holds true.

APPENDIX B: PROOF OF EQ. (16)

The relation in Eq. (16) is shown using the definitions of the angles α and γ.

$$\sin\alpha=z/m, \quad \cos\alpha=r_S/m, \tag{B1}$$

$$\sin\gamma=(z-z_R)/l, \quad \cos\gamma=r_R/l. \tag{B2}$$

If these are inserted into Eq. (A7),

$$y=\frac{ml+z(z-z_R)}{r_S r_R}=\frac{1+\dfrac{z(z-z_R)}{ml}}{\dfrac{r_S r_R}{ml}}=\frac{1+\sin\alpha\sin\gamma}{\cos\alpha\cos\gamma}, \tag{B3}$$

which is the relation in Eq. (16).

APPENDIX C: PROOFS OF EQS. (42) AND (43)

For the thin plate case, the wedge index ν equals 0.5, and then the β term in Eq. (1) can be simplified. The quantity $\cosh(\nu\eta)$ is, for the wedge index $\nu=0.5$,

$$\cosh\frac{\eta}{2}=\frac{1}{2}\left(\exp\frac{\eta}{2}+\exp\frac{-\eta}{2}\right)=\frac{1}{2}\frac{\exp(\eta)+1}{[\exp(\eta)]^{1/2}}. \tag{C1}$$

Squaring this expression gives

$$\cosh^2\frac{\eta}{2}=\frac{1}{4}\frac{\exp(2\eta)+2\exp(\eta)+1}{\exp(\eta)}. \tag{C2}$$

The expression for η in Eq. (A1) can be employed, which readily leads to the simplification

$$\cosh^2\frac{\eta}{2}=\frac{y+1}{2}. \tag{C3}$$

The auxiliary quantity y can then be written as in Eq. (B3), which yields

$$\cosh^2\frac{\eta}{2}=\frac{1+\sin\alpha\sin\gamma+\cos\alpha\cos\gamma}{2\cos\alpha\cos\gamma}=\frac{1+\cos(\alpha-\gamma)}{2\cos\alpha\cos\gamma}$$
$$=\frac{\cos^2[(\alpha-\gamma)/2]}{\cos\alpha\cos\gamma}. \tag{C4}$$

Then, $\cosh(\eta/2)$ can finally be expressed as

$$\cosh\frac{\eta}{2}=\frac{\cos[(\alpha-\gamma)/2]}{(\cos\alpha\cos\gamma)^{1/2}}, \tag{C5}$$

which is the form in Eq. (42). Taking the square root of the right-hand term in Eq. (C4) is safe, as α and γ are always within the range $-\pi/2$ to $\pi/2$. Furthermore, the sine and cosine terms in the expression for β in Eq. (1) can be simplified, since

$$\sin[\nu(\pi\pm\theta_S\pm\theta_R)]=\sin\{[\pi\pm(\theta_S\pm\theta_R)]/2\}$$
$$=\cos[(\theta_S\pm\theta_R)/2], \tag{C6}$$
$$\cos[\nu(\pi\pm\theta_S\pm\theta_R)]=\cos\{[\pi\pm(\theta_S\pm\theta_R)]/2\}$$
$$=\pm\sin[(\theta_S\pm\theta_R)/2], \tag{C7}$$

and allows the β term to be written as

$$\beta(\alpha,\gamma,\theta_S,\theta_R)=\frac{\cos[(\theta_S+\theta_R)/2]}{\cosh(\eta/2)+\sin[(\theta_S+\theta_R)/2]}$$
$$+\frac{\cos[(\theta_S-\theta_R)/2]}{\cosh(\eta/2)+\sin[(\theta_S-\theta_R)/2]}$$
$$+\frac{\cos[(\theta_S-\theta_R)/2]}{\cosh(\eta/2)-\sin[(\theta_S-\theta_R)/2]}$$
$$+\frac{\cos[(\theta_S+\theta_R)/2]}{\cosh(\eta/2)-\sin[(\theta_S+\theta_R)/2]}$$
$$=2\cosh(\eta/2)$$
$$\times\left\{\frac{\cos[(\theta_S+\theta_R)/2]}{\cosh^2(\eta/2)-\sin^2[(\theta_S+\theta_R)/2]}\right.$$
$$\left.+\frac{\cos[(\theta_S-\theta_R)/2]}{\cosh^2(\eta/2)-\sin^2[(\theta_S-\theta_R)/2]}\right\}, \tag{C8}$$

where $\cosh(\eta/2)$ is given in Eq. (C5), and this is the form in Eq. (43).

[1] M. A. Biot and I. Tolstoy, ''Formulation of wave propagation in infinite media by normal coordinates with an application to diffraction,'' J. Acoust. Soc. Am. **29**, 381–391 (1957).
[2] H. Medwin, ''Shadowing by finite noise barriers,'' J. Acoust. Soc. Am. **69**, 1060–64 (1981).
[3] H. Medwin, E. Childs, and G. M. Jebsen, ''Impulse studies of double diffraction: A discrete Huygens interpretation,'' J. Acoust. Soc. Am. **72**, 1005–1013 (1982).
[4] J. P. Chambers and Y. H. Berthelot, ''Time-domain experiments on the diffraction of sound by a step discontinuity,'' J. Acoust. Soc. Am. **96**, 1887–1892 (1994).
[5] D. Ouis, ''Scattering by thin strip-like elements and applications in room acoustics,'' Dissertation, Report TVBA-1005, Lund University of Technology, Lund, Sweden (1995).
[6] A. W. Trorey, ''Diffractions for arbitrary source–receiver locations,'' Geophysics **42**, 1177–1182 (1977).
[7] J. R. Berryhill, ''Diffraction response for nonzero separation of source and receiver,'' Geophysics **42**, 1158–1176 (1977).
[8] Y. Sakurai and K. Nagata, ''Sound reflections of a rigid plane and of the live end composed by those panels,'' J. Acoust. Soc. Jpn. (E) **2**, 5–14 (1981).
[9] G. M. Jebsen and H. Medwin, ''On the failure of the Kirchhoff assumption in backscatter,'' J. Acoust. Soc. Am. **72**, 1607–11 (1982).
[10] G. V. Norton, J. C. Novarini, and R. S. Keiffer, ''An evaluation of the Kirchhoff approximation in predicting the axial impulse response of hard and soft disks,'' J. Acoust. Soc. Am. **93**, 3049–3056 (1993).
[11] R. S. Keiffer, J. C. Novarini, and G. V. Norton, ''The impulse response of an aperture: Numerical calculations within the framework of the wedge assemblage method,'' J. Acoust. Soc. Am. **95**, 3–12 (1994).
[12] A. D. Pierce, ''Diffraction of sound around corners and over wide barriers,'' J. Acoust. Soc. Am. **55**, 941–955 (1974).
[13] R. G. Kouyoumjian and P. H. Pathak, ''A uniform geometrical theory of diffraction for an edge in a perfectly conducting surface,'' Proc. IEEE **62**, 1448–1461 (1974).
[14] C. S. Clay and W. A. Kinney, ''Numerical computations of time-domain diffractions from wedges and reflections from facets,'' J. Acoust. Soc. Am. **83**, 2126–2133 (1988).
[15] W. A. Kinney, C. S. Clay, and G. A. Sandness, ''Scattering from a corrugated surface: Comparison between experiment, Helmholtz–Kirchhoff theory, and the facet ensemble method,'' J. Acoust. Soc. Am. **73**, 183–194 (1983).
[16] J. Vanderkooy, ''A simple theory of cabinet edge diffraction,'' J. Aud. Eng. Soc. **39**, 923–933 (1991).
[17] J. J. Bowman and T. B. A. Senior, *Electromagnetic and Acoustic Scattering by Simple Shapes*, edited by J. J. Bowman, T. B. A. Senior, and P. L. E. Uslenghi (North-Holland, Amsterdam, 1969), Chap. 6.
[18] T. Kawai, ''Sound diffraction by a many sided barrier or pillar,'' J. Sound Vib. **79**, 229–242 (1981).
[19] T. J. Cox and Y. W. Lam, ''Evaluation of methods for predicting the scattering from simple rigid panels,'' Appl. Acoust. **40**, 123–140 (1993).
[20] B.-I. Dalenbäck, ''Room acoustic prediction based on a unified treatment of diffuse and specular reflection,'' J. Acoust. Soc. Am. **100**, 899–909 (1996).